Stapp Car Crash Journal, Vol. 48 (November 2004), pp. 279-299
Copyright © 2004 The Stapp Association

2004-22-0013

Mechanical Properties and Anthropometry of the Human Infant Head

Michael T. Prange, Jason F. Luck, Alan Dibb, Chris A. Van Ee*, Roger W. Nightingale, and Barry S. Myers
Injury and Orthopaedic Biomechanics Laboratory, Duke University
*Design Research Engineering, Novi, MI

ABSTRACT – The adult head has been studied extensively and computationally modeled for impact, however there have been few studies that attempt to quantify the mechanical properties of the pediatric skull. Likewise, little documentation of pediatric anthropometry exists. We hypothesize that the properties of the human pediatric skull differ from the human adult skull and exhibit viscoelastic structural properties. Quasi-static and dynamic compression tests were performed using the whole head of three human neonate specimens (ages 1 to 11 days old). Whole head compression tests were performed in a MTS servo-hydraulic actuator. Testing was conducted using nondestructive quasi-static, and constant velocity protocols in the anterior-posterior and right-left directions. In addition, the pediatric head specimens were dropped from 15cm and 30cm and impact force-time histories were measured for five different locations: vertex, occiput, forehead, right and left parietal region. The compression stiffness values increased with an increase in velocity but were not significantly different between the anterior-posterior and right-left directions. Peak head acceleration during the head impact tests did not significantly vary between the five different impact locations. A three parameter model that included damping represented the pediatric head impact data more accurately than a simple mass-spring system. The compressive and impact stiffness of the pediatric heads were significantly more compliant than published adult values. Also, infant head dimensions, center of gravity and moment of inertia (Iyy) were determined. The CRABI 6-month dummy impact response was similar to the infant cadaver for impacts to the vertex, occiput, and forehead but dramatically stiffer in lateral impacts. These pediatric head anthropomorphic, compression, and impact data will provide a basis to validate whole head models and compare with ATD performance in similar exposures.

KEYWORDS – head injury, skull fracture, pediatric, children, ATD, CRABI, fall

INTRODUCTION

Traumatic brain injury is the most common cause of death in childhood (CDC 1990). Brain injuries resulting in hospitalization or death occur in at least 150,000 children per year, at a rate of over 200 per 100,000 children. Head injury in infancy results in higher morbidity and mortality than that seen in older children (Luerssen 1993). Head injuries cause approximately 75% of the pediatric hospitalizations due to trauma and approximately 30% of childhood injury deaths are caused by head injury (Kraus et al. 1990; James 1999). Ten percent of children suffer from a significant head injury at some point during their school years (James 1999).

Head injuries constitute a greater proportion of all injuries in the infant population (≤1year old) than older children and infants have a greater likelihood of having an intracranial injury after following blunt head trauma (Burdi et al. 1969; Gotschall and Luchter 1999; Greenes and Schutzman 1999). The percentage of infant skull fractures are approximately double that of any other pediatric age group (Gotschall and Luchter 1999). The majority of accidental pediatric head injuries involve motor vehicle collisions (Kraus et al. 1990; Gotschall and Luchter 1999; James 1999).

Since the mid 1980s, much of the basic biomechanics of the head have been studied and the findings published in peer-reviewed journals. Quantitative geometric, constitutive, and structural data are available for the adult head and computational methods are progressing rapidly. Despite this increase in understanding, the mechanical properties of the pediatric head are all but unknown. As an example, recent helmet standards for children have been forced to use adult criteria owing to a lack of pediatric tolerance data (Myers 1997).

One factor that makes pediatric head injury unique is that children are not miniature adults. Children have bodies with different geometric and mass proportions as compared to adults. In a study by Burdi et al., the shape of the human body was examined from birth

until adult age (Burdi et al. 1969). At birth the head makes up about 1/4 of the infants total height and decreased to 1/7 at adulthood. Also at birth, the child has a long trunk with the upper limbs longer than the lower limbs and as the child grows these proportions change drastically (Burdi et al. 1969).

The pediatric skull differs from that of the adult owing to differences in geometry and materials. The newborn has a high and slightly protruding forehead and the infant cranium is longer and rounder than the adult head. The pediatric cranial bones are thin, pliable plates composed of partially calcified bony tissue with an immature diploe. The cranial bones of a child are separated by relatively broad syndesmotic sutures. Fontanelles are located at the junction of these sutures with the most prominent "soft spot" located in the frontal region of the top of the skull. These fibrous tissue sutures allow the skull to expand to accommodate the rapidly growing brain and birthing process. The sutures generally fuse by age two and the anterior fontanelle closes at approximately 2.5 years of life (Ridgway and Weiner 2004).

Several studies relate pediatric animal surrogates to the human child to validate the use of the animal models. Usually the correlation of the pediatric surrogate to the human child is based on a developmental relationship of a shared biological structure or set of structures but again definitive human data are absent (Dobbing 1981; Prasad and Daniel 1984; Thibault and Margulies 1998; Margulies and Thibault 2000). Margulies and Thibault investigated the rate and age dependency of porcine skulls by testing samples of cranial bone and suture to failure in bending (Margulies and Thibault 2000). Unfortunately, the authors were only able to examine one full-term human infant specimen for validation.

Comprehensive studies of mechanical properties of human adult skull and cranial bone have been performed (Hodgson et al. 1967; Hodgson and Patrick 1968; Thomas et al. 1968; Hubbard 1971; Hubbard et al. 1971; McElhaney et al. 1976; Ono et al. 1980). These studies tested the human adult cranial bone in tension, compression, simple shear, and torsion. Unfortunately, there have been few works that attempt to quantify the mechanical properties of the human pediatric skull (McPherson and Kriewall 1980; Kriewall et al. 1981; Margulies and Thibault 2000). These few studies found infant cranial bone stiffness to be approximately 10% of adult cranial bone. Despite these positive contributions, impact, viscoelastic, and quasi-static data on selected age groups are still needed to validate surrogate models and devices.

Along with the lack of data regarding the mechanical properties of the pediatric head, little documentation of detailed pediatric anthropometry exists. Data exist on the anatomical dimensions of children at various ages but no studies have investigated the location of the head center of gravity or quantified the head moments of inertia (Schneider et al. 1986).

Because of this paucity of pediatric data, scaling methods have been employed to determine the head injury tolerance of the child based on adult data (Ommaya et al. 1967; Mertz et al. 1989; Melvin 1995; Irwin and Mertz 1997). These analytical scaling techniques are based on differences in head size, head mass, cranial bone stiffness, and brain stiffness. To date, little human pediatric data exist to benchmark these scaling techniques.

Currently, the biomechanical response of the human infant head is unknown. This paper reports the compressive and impact response using infant cadavaric specimens and derives lumped parameter estimates of infant head structural properties. We hypothesize that the properties of the human pediatric skull differ from the human adult skull and exhibit viscoelastic structural properties. The compression and impact response of a 6-month old anthropomorphic test dummy were measured and compared to the infant cadaver results.

METHODS

Specimen procurement and preparation

Human pediatric cadaver specimens were used to determine the static and dynamic properties of the whole infant head. These biomechanical tests were conducted using three unembalmed fresh-frozen human infant specimens of ages 1, 3, and 11 days after birth. The head was separated from the cervical spine and the mandible was removed while keeping the scalp intact. Maximum head length and maximum head breadth for each specimen were measured using a spreading caliper. After the experimental protocol was complete, the scalp was dissected and the skull was examined for fractures or other tissue damage. The use of pediatric cadaveric tissue was approved by the Duke University IRB.

Anthropometry

Each of the three specimens was imaged using high resolution computed tomography (CT). With the use of cadaveric tissue, these scans could be taken with the highest voltage and current settings (140 kV, 400 mA). This resulted in detailed scans at 0.43 mm/pixel resolution with a slice thickness of 0.625mm at 0.625mm intervals. The CT data was imported into the Amira™ software package (TGS, Inc., San Diego CA) to perform a three-dimensional reconstruction of the head anatomy. The coordinate system for this reconstruction was orientated such that the Frankfort plane was horizontal, the midsagittal plane was vertical, and the origin was located at the level of the superior margin of the right audiory meatus in the midsagittal plane. Head height (auditory meatus to vertex), facial height, and bizygomatic diameter were measure from the CT reconstruction. Locations of the most anterior and most posterior point on the right occipital condyle were determined and the center of the condyle was defined as the average of these coordinates.

After the testing protocol described below was complete, the mandible was reattached using surgical sutures. A pin was inserted into the superior margin of the right auditory meatus and right infraorbital foramen to identify the Frankfort plane. The center of gravity (Cg) of the head was determined using the method described by Walker et al (Walker et al. 1973). Two screw hooks were placed in the skull in the midsagittal plane. If a hook could not be secured in the compliant pediatric skull then a suture was placed through the scalp and used as the attachment point. The mass of the head with mandible and hooks was recorded. The head was suspended in the frame by one of the hooks and a digital image was taken of the right side of the head. A ruler and plumbline were included in the image to establish a scale and vertical direction. Another image was taken with the head suspended by the other hook. The location of the hooks, superior margin of the auditory meatus, infraorbital foramen, and plumbline were digitized from each image (Scion Image, Scion Corporation). The two images were registered by aligning the auditory meatus and Frankfort plane of each image. The Cg of the head was determined by the location of the intersection of the vertical lines passing through the suspension point of each image (Walker et al. 1973).

While suspended, the head was swung in the midsagittal plane. The motion of the head was recorded with a digital video camera at 50Hz and the period of the swing (T) was measured. The period of the motion was determined as the average period over the first 10 swings. The error of the measured period using this method was approximately ± 2 msec. The mass moment of inertia about the y-axis (line in the transverse direction, I_{yy}) at the Cg was calculated using the mass moment of inertia of the pendulum at its suspension point and the parallel axis theorem:

$$I_{yy} = \frac{mgdT^2}{4\pi^2} - md^2 \qquad (1)$$

where m is the mass of the head, g is the acceleration due to gravity, and d is the distance from the Cg to the suspension point (Walker et al. 1973). The mass of the hooks were less than 0.2% of the mass of the head therefore the hooks' moments of inertia were considered negligible.

Pediatric head compression

Experimental protocol- A series of compression tests were conducted to determine static and rate-dependent properties of the infant head in two directions. The maximum head deformation during the compression was limited to 5% of the total gauge length of the head in order to ensure that no damage or fractures occurred. The foramen magnum was loosely blocked with gauze to contain the intracranial contents prior to testing while imposing negligible resistance to extrusion during the experiments.

Using a parallel plate fixture and MTS hydraulic actuator, force-deflection data was recorded during whole head compression experiments. A uniaxial strain gauge load cell (S-type, Omega Engineering Inc.) was used to measure the compressive load and a LVDT was used to measure the position of the actuator. Data for all tests were recorded using a digital data acquisition system (National Instruments, Austin, TX). The head was positioned between the two smooth flat plates so that the compression direction was in the anterior-posterior (AP) or right-left (RL) direction and along the Frankfort plane. At the beginning of the experiment the actuator was adjusted to achieve approximately 0.5N of pre-compressive force. This pre-compressive force was necessary to maintain the specimen between the plates in the correct orientation. Before each test the head was repositioned and the gauge length was measured if necessary.

Prior to the test battery, the head was preconditioned at 50% of maximum displacement at 1 Hz for 60 seconds. The head was compressed at a constant velocity using four different rates. A test was conducted at 0.05 mm/s to determine the quasistatic

stiffness of the head. Three additional compression tests were conducted to the same displacement at constant velocities of approximately 1.0 mm/s, 10 mm/s, and 50 mm/s. These experiments were conducted in the AP and RL directions. Because of limitations of the hydraulic actuator, the 50 mm/s velocity tests resulted in the varying velocity during the end of the test. Therefore, this non-constant velocity data from the last 1 mm of displacement during these high rate experiments were omitted from the analysis. Also, the 50 mm/s tests were not recorded for the 11 day old specimen due to data acquisition errors during the experiment.

Analysis - Because the force-deflection data was nonlinear, each test was regressed between 50% through 100% maximum displacement in order to determine a stiffness value. The slope of this line was defined as the stiffness and the x-intercept of the projected line as the low-load displacement. The whole data set was also regressed using an exponential function:

$$F = A\left(e^{Bx} - 1\right) \tag{2}$$

where A and B are constants and F and x are the compressive force and displacement respectively. These analyses were repeated for each of the two compression directions and each of the four velocities. An average stiffness, low-load displacement, A, and B across specimens were calculated for each compression direction and velocity. Differences between direction and velocity were determined using 2-way analysis of variance (ANOVA) and Tukey tests for multiple comparisons. The significance level for the statistical analysis was set at 5%. Also, the coefficient of determination (r^2) values of the linear and exponential regression for each experiment were compared using a paired Student's t test.

Pediatric head impact

Experimental protocol – After the compression experiments were complete, voids in the cranial cavity were filled with water and the foramen magnum was sealed tightly with polymethylmethacrylate (PMMA) to contain the intracranial contents during the impact tests. The mass of the head was then measured and recorded. The head was held in a net and suspended by a string at a prescribed height. The head was released by burning the string which allowed the head to free fall in its original orientation without initial translation or rotation onto a flat smooth anvil. The force-time history was recorded by a Kistler 3-axis piezoelectric load cell and data were recorded using a digital acquisition system at 10,000 Hz (3 day old specimen) or 100,000 Hz (1 and 11 day old specimens). Each head was impacted at approximately 15cm and 30 cm drop heights. The actual height of each drop test was measured using a ruler. At each of these drop heights the head was impacted once on each of five locations: vertex, occiput, forehead, right parietal bone, and left parietal bone. All tests were conducted nondestructively so that the head specimens could be used in subsequent experiments.

Analysis - Each impact was digitally filtered according to the SAE J211b Class 1000 filter specifications for head impact. Acceleration of the head was calculated by dividing the force data by the measured head mass. Peak acceleration, pulse duration, and the head injury criterion (HIC) were calculated from the acceleration-time data. Pulse duration was defined from the first point where the impact force was greater than 5 N and the point where the force trace returned to zero. An average peak acceleration, duration, and HIC were calculated for each impact location and each height. Differences between location and height were determined using 2-way analysis of variance (ANOVA) and Tukey tests for multiple comparisons. The significance level for the statistical analysis was set at 5%.

Analytical models of pediatric head impact

The head impact data was represented by two different mathematical models. First, the force-time data was modeled as a simple mass-spring system. The governing equation of this system is:

$$m\ddot{x} + kx = 0 \tag{3}$$

where m is the head mass, x is the head displacement during impact, $\ddot{x}$ is the acceleration of the head during impact, and k is the stiffness of the spring.

The second method of representing the head impact data involved coupling a head mass to a three parameter viscoelastic model. This model consisted of one spring in parallel with another spring and dashpot that are in series (Figure 1). This model has been used previously to describe the stress relaxation and creep behavior of biological tissues (Fung 1993). During an impact after free fall, the behavior of this viscoelastic system is described by the following differential equation:

$$\dddot{x} + \frac{k_2}{c}\ddot{x} + \left(\frac{k_2}{m} + \frac{k_1}{m}\right)\dot{x} + \frac{k_1 k_2}{c\,m}x = 0 \tag{4}$$

where k_1 and k_2 are the spring constants and c is the coefficient of viscosity of the dashpot.

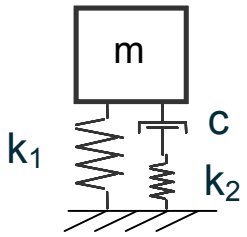

Figure 1: Schematic of three parameter solid model of head impact

For each impact, the spring constant k_1 was determined from the quasi-static (0.05 mm/s) head compression tests for that particular specimen. The value of k_1 for the occiput and forehead impacts was established as the linear stiffness from the quasi-static AP head compression tests. For the right and left parietal region impacts, k_1 was set to the linear stiffness from quasi-static RL direction compression experiments. Because head compression tests were not conducted in the superior-inferior direction, the average linear stiffness between the AP and RL directions were used as the k_1 value for the vertex impact models. The initial velocity of the head for both models was calculated using the measured drop height of the experiment.

These mass-spring and three parameter model differential equations were solved numerically to find the material constants for each drop (Matlab 6.1, The Mathworks, Inc.). The peak force of the measured data and the model solution of each drop were aligned by the half power method (Meirovitch 2001). The solutions of both models were optimized to find the material constants that minimize the residual sum of squares between the model solution and the measured data. The coefficient of determination (r^2) of the regressions used to determine the material constants were reported as well as the absolute percent error of the predicted peak head acceleration. The r^2 values of the three parameter model and mass-spring system solutions for each experiment were compared using a paired Student's t test.

For each specimen, a spring constant (k) and c and k_2 of the three parameter solid were found for each impact test. The relaxation time constant for the three parameter model was calculated as:

$$\tau_x = \frac{c}{k_2} \qquad (5)$$

An average value for the spring constant and three parameter model time constant were averaged across height and impact location. Differences between each of these parameters were determined using 2-way analysis of variance (ANOVA) and Tukey tests for multiple comparisons. The significance level for the statistical analysis was set at 5%.

To validate the three parameter model, two sets of predictions were made and compared to the measured data. First, the force-time data of each 15 cm drop test were calculated using the material constants found from the 30cm drop data for the same specimen and impact location. Second, the material constants for the same specimen and impact location determined from the 15cm drop data were used to predict the force-time data of each 30cm drop. The predicted response and the measured data of each set of predictions were compared by determining r^2 for the pulse and absolute percent error of the calculated peak head acceleration. A Student's t test was used to compare differences between the r^2 values and peak acceleration error of the two prediction methods.

Anthropomorphic dummy head impact and compression

Experimental protocol- A series of drop tests were conducted to determine the impact response of the head of a Child Restraint and Airbag Interaction (CRABI) 6-month old anthropomorphic test device (ATD). Compression tests of the ATD head were performed to determine its static and dynamic structural properties. The CRABI head was compressed at 4 different constant velocities using the same protocol described above for the cadaver specimens. The dummy head was compressed to approximately the same forces measured in the cadaver experiments. The head was compressed in both the AP and RL directions.

Drop tests were also performed using the same protocol and instrumentation described above for the cadaver specimens. The head impacted a flat smooth anvil and the force-time history was recorded by a Kistler 3-axis piezoelectric load cell. The impact response was measured after drops from 15 and 30 cm onto 5 different impact sites on the head.

Analysis - As in the cadaver compression data analysis, each compression test was regressed between data taken from 50% through 100% maximum displacement in order to determine a stiffness value. The slope of this line was defined as the stiffness and the x-intercept as the low-load displacement. These analyses were repeated for each of the two compression directions and each of the

four velocities. An average stiffness and low-load displacement were calculated for each compression direction and velocity.

Each impact was digitally filtered according to the SAE J211b Class 1000 filter specifications for head impact. An average peak acceleration (peak force divided by head mass) and HIC were calculated for each impact location and each height. Differences between location and height were determined using 2-way ANOVA and Tukey tests for multiple comparisons.

RESULTS

Anthropometry

The average maximum head length, maximum head breadth, and head mass with mandible attached were 10.8 cm, 9.2 cm, and 620 grams respectively. The average location of the head center of gravity (Cg) was 0.4 cm anterior and 2.3 cm superior from the superior margin of the auditory meatus. The average location of the center of the occipital condyle was 1.4 cm posterior and 2.8 cm inferior from the Cg of the head. Average mass moment of inertia about the y-axis (line in the transverse direction) at the Cg was 4945 $gm \cdot cm^2$. All anthropomorphic measurements for the three specimens are reported in Table A1.

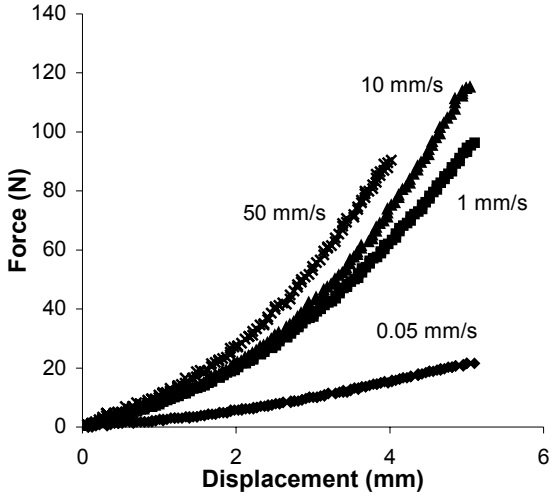

Figure 2: Typical infant cadaver force-deflection curves for head compressions at four different velocities in the AP direction (3 day old specimen).

Pediatric head compression

The force-deflection data for all tests displayed an initial toe region with increasing stiffness at the higher displacements (Figure 2). The linear regression of the data from 50% to 100% maximum deflection fit the data well with and an average r^2 of 0.992 (Table A2). The exponential model also fit all the individual responses well with an average r^2 of 0.998. A paired Student's t-test revealed that the r^2 value was significantly improved with an exponential fit ($p<0.001$), however this difference is only 0.01 on average.

Statistical analysis revealed that the linear stiffness was dependent on deflection velocity ($p<0.01$) The average stiffness values for the 0.05, 1.0, 10, and 50 mm/s constant velocity compression tests were 7.45, 23.3, 29.9, and 29.5 N/mm respectively (Table A2, Figure 3). The quasi-static (0.05mm/s) stiffness was significantly less than the three higher rates however the 1.0, 10 and 50 mm/s stiffness values were not significantly different from each other. A change of velocity over thee orders of magnitude (0.05 to 50 mm/s) increased the stiffness by a factor of four. Over a one order magnitude change of velocity from 1.0 to 10 mm/s. the stiffness increased only by a factor of 1.3 but this change was not statistically significant.

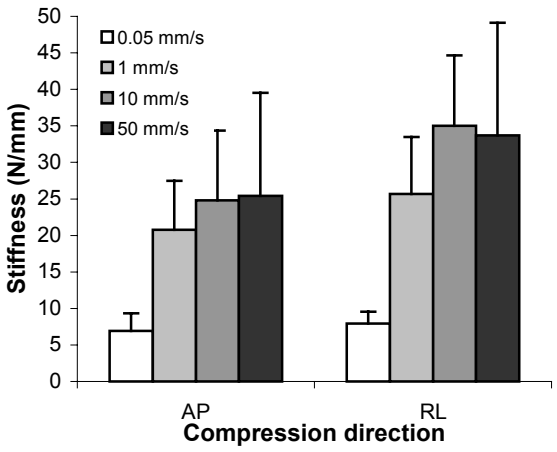

Figure 3: Stiffness values determined from head compression tests at different constant velocities in two different directions. The stiffness value determined from the quasi-static (0.05 mm/s) tests was significantly less than the three other higher velocities. Stiffness did not demonstrate a dependence on compression direction. Error bars indicate standard deviation.

The average low load displacement also showed dependence on the loading rate ($p<0.01$). The average low load displacement across both directions for the 0.05, 1.0, 10, and 50 mm/s constant velocity compression tests were 1.1, 1.6, 1.6, and 1.2 mm respectively (Table A2). The quasi-static low load displacements were statistically different from the 1.0 and 10 mm/s experiments however this difference was only 0.5mm on average.

Stiffness and low load displacement did not demonstrate a dependence on compression direction. The average stiffness and low load displacement for anterior-posterior (AP) direction across all velocities were 18.9 N/mm and 1.40 mm respectively (Table A2). The average stiffness, and low load displacement for the right-left (RL) direction across all velocities were 24.8 N/mm and 1.39 mm respectively. The stiffness and low load displacement were not significantly difference between the two compression directions ($p>0.12$, Figure 3).

Pediatric head impact

Peak acceleration and HIC varied with drop height but did not change between impact location (Table A3, Figure 4). Average peak acceleration and HIC during the 30cm drop height impacts were 55.3 g and 84.1 respectively. Both these average values were significantly greater than the average peak acceleration and HIC values of 38.9 g and 32.9 respectively for the 15cm drop height impacts ($p<0.001$, Figure 5). The acceleration pulse durations were not significantly different between the 15 cm and 30cm drop height impacts with an average pulse duration of 18.3 msec.

Peak acceleration and HIC measurements were not significantly different between any of the impact location sites ($p=0.18$ and $p=0.78$, Table A3). The peak acceleration and HIC for the impacts on the vertex were greater but not significantly different than impacts on the occiput, forehead, left and right parietal regions (Figures 6-7). Average pulse duration was longer for the vertex impacts, but again this difference was not statistically significant ($p=0.89$). After all testing was complete, the specimens were dissected and no skull fractures or other permanent deformation was identified.

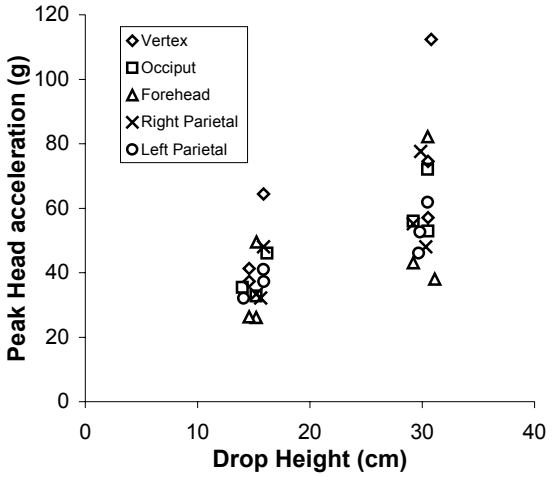

Figure 4: Peak acceleration and drop height for all infant cadaver impact tests.

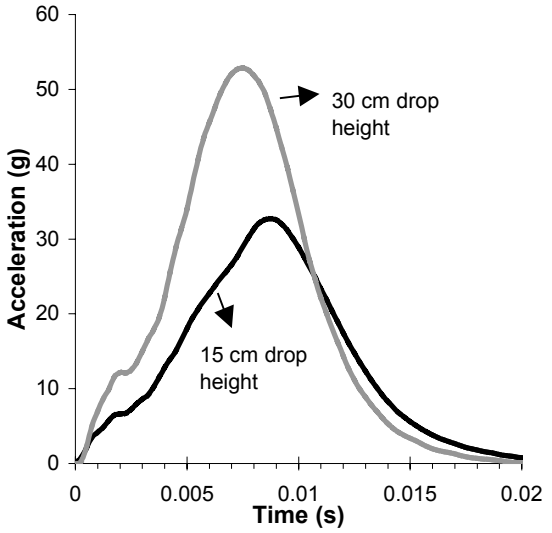

Figure 5: Typical infant cadaver head acceleration pulses from two different drop heights onto the same impact location (occiput, 11 day old specimen).

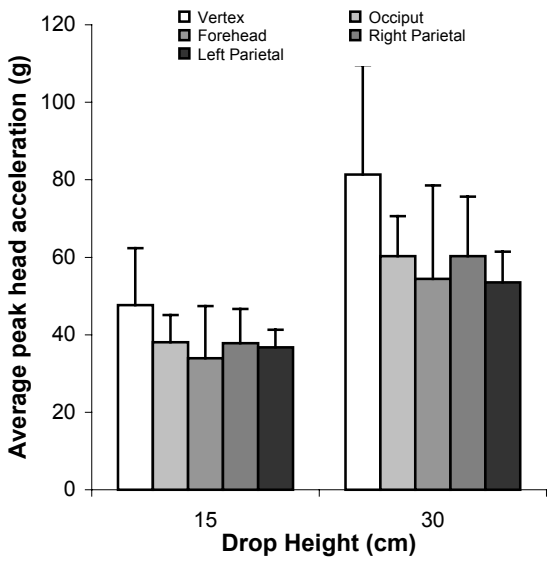

Figure 6: Average peak head acceleration at each height and impact location. Average peak accelerations were significantly different between drop height but did not vary between impact locations. Error bars indicate standard deviation.

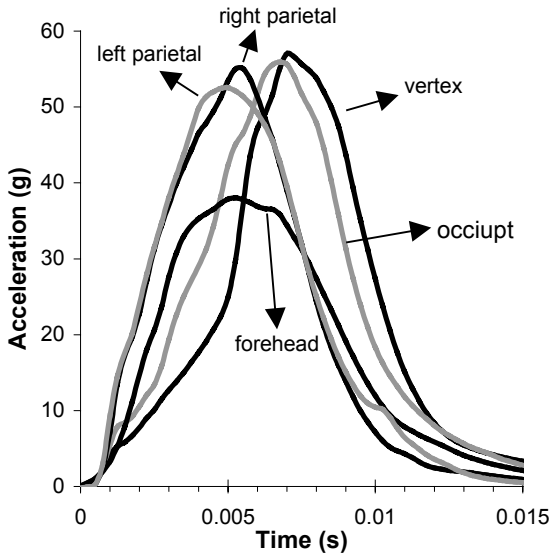

Figure 7: Typical infant cadaver head acceleration pulses from the same drop height (30 cm) onto the five different impact locations (1 day old specimen).

Analytical models of pediatric head impact

The mass-spring model was unable to fully represent the measured impact data (Figure 8). The average r^2 value across all tests was 0.81 ranging from 0.71 to 0.89. The absolute percent error of the predicted peak head acceleration was 16% on average with 21 out of 30 impact models over estimating the peak acceleration. The pulse duration of the model was shorter than the cadaver data for all impacts with a average percent error of 28%. Statistical analysis revealed that the spring constant (k) did not significantly change with impact location but did show a dependence with drop height (Table A4). The values of k the occipital impacts were slightly lower than the other four locations but this difference was not statistically significant ($p=0.663$). The spring constant for the 30cm drop heights were an average of 1.4 times greater than the 15cm impacts ($p<0.05$). The average spring constant across all impact locations was 29.4 N/mm for the 15cm drops and 41.1 N/mm for the 30cm drops.

The three parameter model resulted in a better representation of the impact data than the mass-spring system (Figure 8). The average r^2 value for the three parameter model was 0.93 with a range of 0.83 to 0.98. Twenty eight out of the thirty impact models under estimated the peak head acceleration resulting in an average absolute percent error of 9.5%. The absolute percent error of the predicted pulse duration was 36% on average with all the impacts models predicting shorter durations than the cadaver data. The r^2 values for the three parameter models were significantly greater than the r^2 values for the mass-spring fit in every test with an average increase of 0.12.

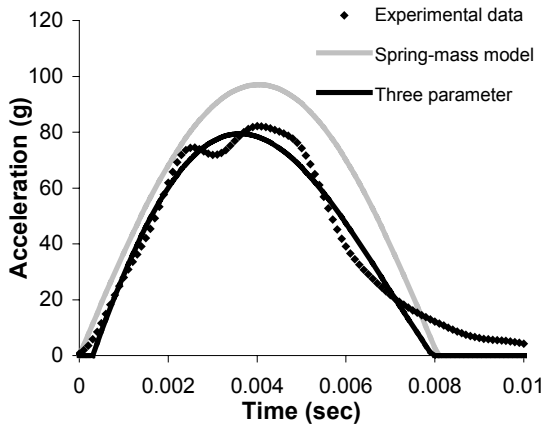

Figure 8: Typical infant cadaver head acceleration pulses with corresponding mass-spring and three parameter model estimations (3 day old specimen, forehead impact from 30 cm).

The relaxation time constant did no showed a dependence on impact location and drop height (Table A5). The average values of τ_x in the vertex impacts were less than the other locations however this was not statistically different (p=0.23). The time constant for the 30 cm drops were shorter than the 15 cm drops but this difference was not significant (p=0.45).

The three parameter model was able to predict the measured data of one height given the parameters determined from the other drop height. Using the k_1, k_2 and c values for the 15cm impacts of each specimen and location, the predicted 30cm impacts resulted in an average r^2 value of 0.87. The absolute percent error of the predicted peak acceleration was 19% on average. The predicted 15cm impacts using the 30cm drop height parameters resulted in higher r^2 values ($p<0.01$) and lower peak acceleration errors ($p<0.001$) when compared to the first set of predictions. This second method of predicting the lower height impact response from the higher height impact model parameters showed an average r^2 value of 0.92 with an average absolute peak acceleration error of 7.1%.

Anthropomorphic dummy head impact and compression

ATD peak acceleration and HIC varied with drop height and impact location (Table A6). Peak acceleration during the CRABI 30 cm drop height impacts onto the vertex, occiput, forehead, right parietal and left parietal region were 51.8, 61.6, 84.8 144.9, and 214.5 g respectively. Impacts from 15 cm revealed peak accelerations of 33.8, 39.5, 37.3, 66.8, and 116.0 g onto the vertex, occiput, forehead, right parietal and left parietal region respectively. These values were significantly less than the peak accelerations for the 30 cm drop height impacts. Also, peak accelerations were significantly higher during the right and left parietal impacts than impacts to the occiput and vertex (Figure 9). Along with the increase in peak acceleration, the acceleration pulse for the right and left parietal impacts were shorter in duration than the other impact location (Figure 10). The dummy behaved similar to a mass-spring system with the pulse duration decreasing only slightly during the 30 cm drop tests.

The linear regression of the compression data fit the data well with and an average r^2 of 0.999. Stiffness of the CRABI head increased with higher compression velocity. The stiffness values for the 0.05, 1.0, 10, and 50 mm/s constant velocity AP compression tests were 18.5, 22.4, 26.4, and 28.7 N/mm respectively (Table A7). The RL compression direction revealed stiffness values of 62.4, 82.9, 95.1 and 95.7 N/mm for 0.05, 1.0, 10, and 50 mm/s constant velocities respectively. The stiffness across all velocities for RL direction was approximately 2.5 times greater on average than the AP direction stiffness (Table A7). The average low load displacement showed little change with loading rate or compression direction.

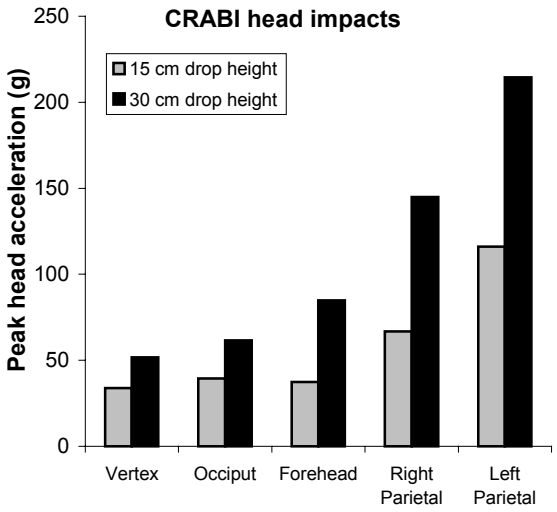

Figure 9: CRABI peak head acceleration for 5 impact locations from 15 cm and 30 cm drop heights. CRABI accelerations increased with drop height and lateral impact accelerations were greater than impacts on the vertex and occiput at both drop heights.

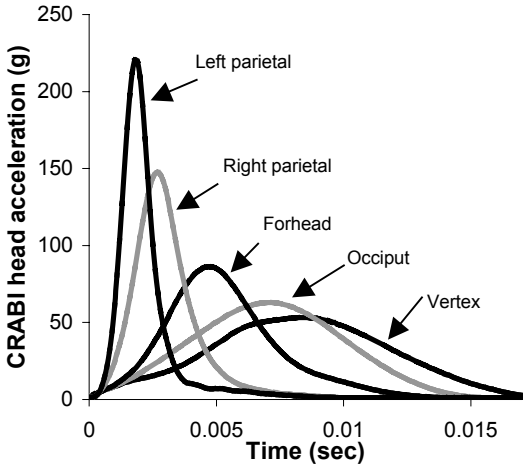

Figure 10: CRABI head accelerations from drop heights of 30cm onto the five different impact locations.

DISCUSSION

Limitations

One limitation of this study is the small number of specimens tested. Because pediatric cadaveric tissue is rarely available, these three specimens represent all the appropriate infant specimens that have been procured. However, with the paucity of pediatric biomechanical data, these experiments provide previously unavailable information about the human infant head dynamic response. Indeed, these pediatric results provide the first set of human head biomechanical data for the validation of scaling methods, animal experiments, computational models, and anthropomorphic dummy biofidelity.

Because pediatric cadaveric tissue is rarely available, this tissue was also used in a series of biomechanical experiments beyond the scope of this paper. For this reason compression and impact tests were conducted on the head specimens at sub-failure loads in order to ensure that no bone fracture or permanent skull deformation occurred. Therefore these studies examine the mechanics at sub-failure levels and do not assess the fracture biomechanics of the pediatric skull. Because no factures occurred as a result of the drop tests, these results indicate that a peak acceleration of 55 g and a HIC value of 84 are below the infant skull fracture tolerance.

Another limitation of these studies is the boundary condition at the foramen magnum during the compression and impacts tests. Normally the brain and spinal cord are surrounded by cerebral spinal fluid (CSF) and the CSF flows between the intracranial cavity and the spinal canal through the foramen magnum. In our experimental protocol the cervical spine was separated from the head during a previous test. Also, the cadaveric tissue was frozen and thawed resulting in significant changes in the brain tissue properties. Previous studies show that the incompressible nature of the intracranial contents significantly affects the head impact response (Klinich et al. 2002). To simulate the incompressible brain material and CSF in our experiments, the head was filled with water and sealed to prevent extrusion of the intracranial contents. Similar methods have been used during adult head impact drop tests to replicate the incompressible nature of the head (Ono et al. 1980).

The head compression tests were conducted at significantly lower rates than impacts conditions. Because the intracranial contents are incompressible, tissue extrusion and CSF flow out of the foramen magnum could be possible during these slow, non-impact deformation rates. To simulate this condition, the foramen magnum was open during the compression tests allowing the free movement of tissue out of the foramen magnum. Adult head compression tests have used a similar method to simulate the in vivo foramen magnum boundary condition (Thomas et al. 1968).

The cadaveric specimens tested in this study were newborn infants and younger than the designed age of the 6-month CRABI dummy. Scaling methods were used to design the child ATD head response based on cranial bone stiffness. Cranial bone has been shown to increase in stiffness from birth to 6-months of age (McPherson and Kriewall 1980; Melvin 1995; Irwin and Mertz 1997). Therefore, according to scaling methods, the predicted CRABI accelerations should be approximately 15% greater than the infant response.

Analytical models of pediatric head impact

This study presents a viscoelastic model to characterize the rate dependent structural properties of the infant head during impact. The three parameter model resulted in a better representation of the infant impact data than a mass-spring model (Figure 8). The three parameter model had a significantly higher r^2 value and lower error in predicting the peak acceleration. The average r^2 value for the mass-spring model was 0.81 demonstrating that the acceleration pulse is not well represented as sine wave that the mass-spring model predicts. However the average r^2 value for the three parameter model was 0.93 showing that this model better represented the shape of acceleration data. The additional parameter afforded the model the opportunity to fit both the magnitude and duration of the acceleration pulse independently for the three parameter model while the both of these parameters are coupled by the spring constant in the mass-spring model. Also, the three parameter model includes a viscous component and can better replicate the damped unloading response observed in the impact data.

Head impact

Comparison of the infant head impact results to previous adult data are complicated because of differences in experimental design and acceleration calculation methods. In some previous impact tests of adult head, accelerometers were attached to the skull and the head acceleration was measured directly. That method was not feasible with the infant specimens because the thin, pliable cranial bone made the fixation of accelerometers to the pediatric skull extremely difficult. Also, because of the broad, compliant sutures joining the cranial bones, the infant skull is not a rigid body and accelerometers would not produce an accurate measurement of head Cg acceleration. Therefore, infant head accelerations during drop tests were calculated using the measured force at impact and the mass of head.

Owing to the difference in acceleration calculation methods, comparison of our infant data were limited to those studies in which head accelerations could be estimated from impact force and average head mass reported in the literature. Average peak acceleration measured in the infant cadaver were 55 g with an average pulse duration of 18 msec during the 30 cm drop tests. Ono et al. reported an average peak head acceleration of 206 g and average duration of 2.2 msec during drops tests of adult heads from more than 40 cm onto a flat anvil that did not result in skull fracture (Ono et al. 1980). Nightingale et al. measured an average peak head acceleration of 167 g and pulse duration of 5 msec during cadaver drop tests from 53 cm (Nightingale et al. 1996). Average peak head acceleration and duration measured by Hodgson and Thomas using a rotating pallet were 172 g and 7msec respectively (Hodgson and Thomas 1971). The equivalent drop height of these tests were an average of 57 cm and all the tests resulted in skull fractures (Hodgson and Thomas 1971; Mertz 1985). All of these adult responses had greater peak acceleration and shorter pulse durations than the infant cadaver head impact response from drop heights greater than the heights used in the infant cadaver protocol. Assuming linearity, while peak acceleration will vary with impact velocity, pulse duration is independent of impact velocity. On this basis, the first-mode vibration frequency of the infant skull is significantly lower than the adult.

Other adult drop tests from similar heights to the pediatric experiments have been reported. Head acceleration from accelerometer data is reported by Hodgson and Thomas at equivalent heights of approximately 15 and 30 cm (Hodgson and Thomas 1971; Mertz 1985). Eight tests were conducted from 15±4 cm resulting in an average peak head acceleration of 107 g. Tests conducted at 30±3cm produced 205 g average peak acceleration with three out of the four tests resulting in skull fracture. Although the adult measurements were taken from accelerometer data, these values are considerably greater than the infant drop test results.

The majority of the adult head data were determined during impact to the forehead of the cadaver. Ono et al. investigated impacts to both the forehead and occiput (Ono et al. 1980). These data show no difference in the peak accelerations between the two impact locations. The infant cadaver also showed no dependence of the response with impact location.

Head compression

The infant cadaver showed an increase in structural head stiffness with an increase in rate of compression and revealed no directional dependence of stiffness over the range of velocities tested. In contrast, Hogdson et al. reported AP stiffness of the adult head during static flat plate compression to be approximately 50% greater than the lateral direction (Hodgson et al. 1967). Thomas et al. also found differences in the volume change due to compression in different directions (Thomas et al. 1968). In contrast, the infant cadaver data did not reveal statistically significant changes in stiffness between the AP and lateral compression at any velocity.

The stiffness values for adult head compression are dramatically different from the infant data. Thomas et al. reported a stiffness of approximately 2975 N/mm during static, point load compression in the AP direction of an adult cadaveric head. Adult stiffness values measured by Hodgson et al. during static compression using flat plates were 1590 N/mm in the AP direction and 1070 N/mm in the lateral direction. Dynamic point load stiffness was reported to by 7360 N/mm. The average compressive stiffness of the infant cadaver head, 22 N/mm, is approximately one to two orders of magnitude less than the adult values. Again, this shows the dramatically more compliant nature of the infant head.

Scaling of adult head impact data

To account for the compliant infant head in the absence of cadaver impact data, scaling techniques have been used to predict the pediatric response. These methods use differences in head size and cranial bone stiffness to scale adult impact data to the child. To examine the validity of these methods, the adult peak acceleration data reported in the literature were scaled using dimensional analysis described by Melvin (1995). Anthropomorphic data and cranial bone stiffness for adult and newborn ages result in ratios of 0.70 and 0.25 for the characteristic head length and skull stiffness respectively (Hubbard 1971; McPherson and Kriewall 1980; Schneider et al. 1986; Irwin and Mertz 1997). The ratio of the accelerations is directly proportional to the ratio of skull bending stiffness and inversely proportional to the characteristic head length ratio (Melvin 1995). Using this method, the adult head impact accelerations outlined above were scaled to the infant resulting in accelerations of 75 to 60 g (Hodgson and Thomas 1971; Ono et al. 1980; Mertz 1985; Nightingale et al. 1996). These adult data were from drop heights greater than the infant cadaver tests (Figure 11). However, the scaled values are only slightly higher than the measured infant cadaver accelerations from drops of 30 cm. Thus, these cadaver data provide support and validity to scaling methods currently in use to predict the infant impact response.

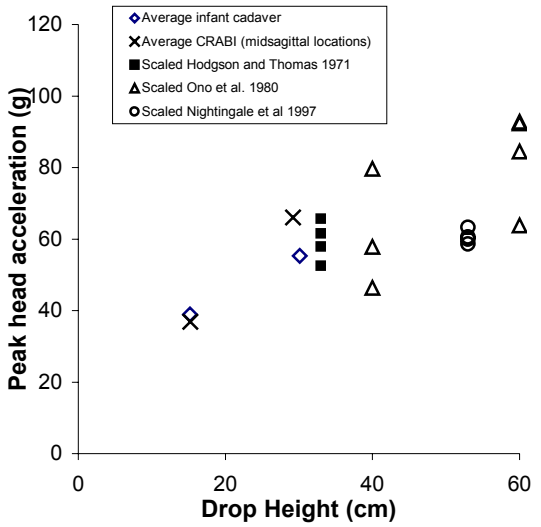

Figure 11: Peak acceleration and drop height for scaled adult cadaver, average CRABI (vertex, occiput, forehead), and average infant cadaver head impact tests. Filled symbols indicate skull fracture occurred as a result of impact and open symbols how non-fracture data.

Comparisons of cadaver and CRABI responses

With the absence of human pediatric cadaver data, scaling methods were used to design the child anthropomorphic test dummies (Irwin and Mertz 1997). To assess the biofidelity of the youngest child dummy, a 6-month old CRABI dummy head was tested using the same protocol as the infant cadaveric tissue. The CRABI head impact response was statistically similar to the cadaver data during the vertex, occiput, and forehead impacts from both 15 cm and 30 cm drops. However, significant differences were found between the lateral impacts when compared to the cadaver data. The peak acceleration and HIC values for the CRABI drops were not significantly different from the cadaver data during impacts onto the vertex, occiput, and forehead at both drop heights (t-test, $p>0.20$, Figures 12-13). The right and left parietal CRABI head impacts resulted in significantly higher peak accelerations and HIC values ($p<0.05$). HIC results were two to five times higher than the cadaver values for these lateral impacts. Both the cadaver and CRABI impacts did not show a change in pulse duration with increasing drop height. Acceleration pulse duration for the CRABI head drops were lower than the corresponding average cadaver response for all impact locations and heights however these differences were not statistically significant.

The compression tests showed similar results as the impact experiments. The CRABI stiffness values for the 1, 10, and 50 mm/s in the AP direction constant velocity tests were statistically similar to the infant cadaver results (Figure 14). In contrast, the dummy RL direction 0.05, 1, and 10 mm/s constant velocity tests were found to be approximately 3 to 8 times stiffer than the infant cadaver experiments (Figure 15). The quasi-static (0.05 mm/s) compression stiffness in both directions were significantly greater than the quasi-static stiffness of the cadaver specimens ($p<0.05$). These data show that the CRABI 6-month dummy behaves similar to the infant cadaver for impacts to the vertex, occiput, and forehead. However, the dummy is dramatically stiffer than the human infant in response to a lateral impact.

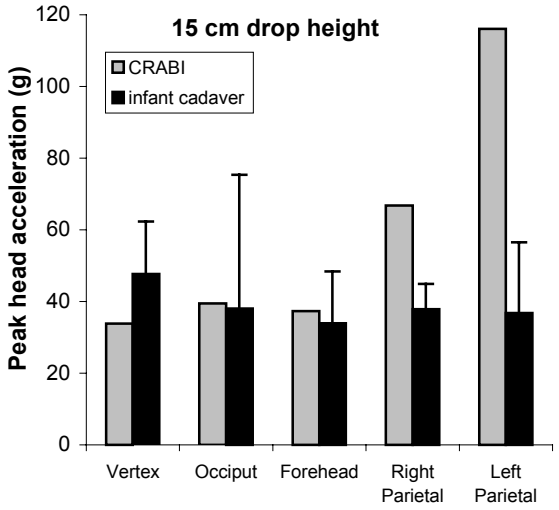

Figure 12: CRABI and infant cadaver peak head acceleration for 5 impact locations from 15 cm drop height. CRABI acceleration was similar to the cadaver data for the vertex, occiput, and forehead impacts but significantly greater for the lateral impact. Error bars indicate standard deviation.

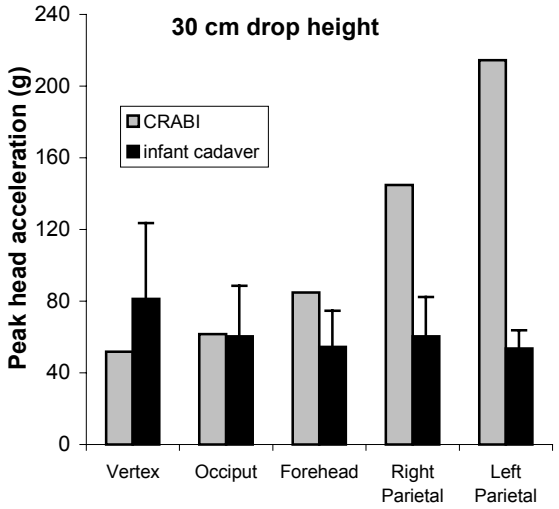

Figure 13: CRABI and infant cadaver peak head acceleration for 5 impact locations from 30 cm drop height. CRABI acceleration was similar to the cadaver data for the vertex, occiput, and forehead impacts but significantly greater for the lateral impact. Error bars indicate standard deviation.

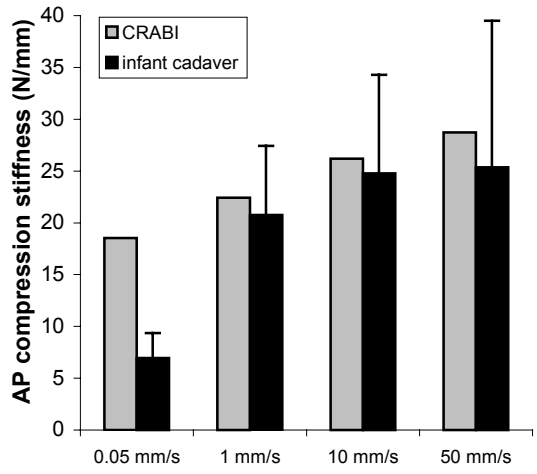

Figure 14: CRABI and infant cadaver head compression stiffness for the four constant velocity tests in the AP direction. CRABI results were statistically similar to the 1, 10, and 50 mm/s cadaver data.

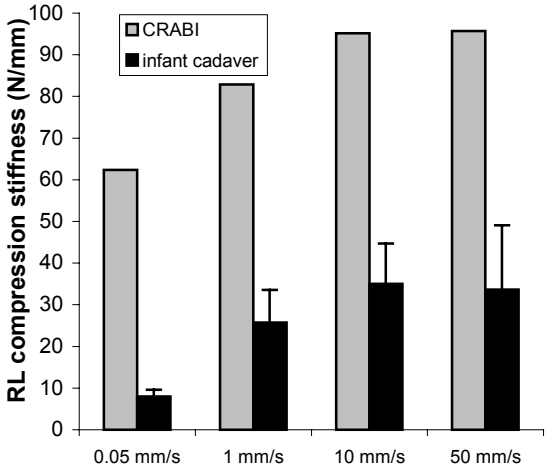

Figure 15: CRABI and infant cadaver head compression stiffness for the four constant velocity tests in the RL direction. CRABI stiffness values were significantly greater to the 0.05, 1, and 10 mm/s cadaver results.

CONCLUSIONS

This study reports the dynamic response, compression structural properties, and anthropometry of the human infant head. Drop tests revealed that the impact response of the infant head showed no dependence on impact location. Also, the structural stiffness of the infant head did not depend on compression direction. The compression tests revealed that the stiffness was dependent on velocity indicating the infant head behaves as a viscoelastic material.

These data show the infant head is dramatically more compliant than the adult. Previous adult head impact data had significantly greater peak acceleration and shorter pulse durations than the infant head impact response. Also the compressive stiffness of the adult cadaver head is considerably greater than the infant values. The infant cadaver impact tests showed similar results as scaled adult data and provide validity to current scaling methods to predict the infant impact response.

These data also show that the CRABI 6-month dummy response is similar to the infant cadaver for impacts to the vertex, occiput, and forehead. However, the dummy is dramatically stiffer than the human infant in response to lateral impacts. These pediatric head anthropomorphic, compression, and impact data will provide a basis to validate whole head models and compare with ATD performance in similar exposures.

ACKNOWLEDGMENTS

Funding for this project was provided by the National Highway Traffic Safety Administration, and the Southern Consortium for Injury Biomechanics at the University of Alabama, Injury Control Research Center. The 6-month CRABI dummy was provided by Wayne State University.

REFERENCES

Burdi, A., Huelke, D., Snyder, R. and Lowrey, G. (1969) Infants and children in the adult world of automobile safety design: pediatric and anatomical considerations for design of child restraints. Journal of Biomechanics 2: 267-280.

CDC (1990) Childhood injuries in the United States. American Journal of Diseases of Children 144(6): 627-46.

Dobbing, J. (1981) The later development of the brain and its vulnerability. In Scientific Foundations of Paediatrics, ed. J. Davis and J. Dobbings, Heinemann Medical, London.

Fung, Y. (1993) Biomechanics: Mechanical Properties of Living Tissues. Springer-Verlag, New York.

Gotschall, C. and Luchter, S. (1999) Head injuries to motor vehicle occupants aged 0-5 years. Proc. Child occupant protection in motor vehicle crashes session. AAAM and IRCOBI, pp. p17-27. Professional Engineering Publishing.

Greenes, D. S. and Schutzman, S. A. (1999) Clinical indicators of intracranial injury in head-injured infants. Pediatrics 104(4 Pt 1): 861-7.

Hodgson, V., Gurdjian, E. and Thomas, L. (1967) Development of a model for the study of head injury. Proc. 11th Stapp Car Crash Conference, pp. 432-443. Society of Automotive Engineers, Warrendale, PA.

Hodgson, V. and Patrick, L. (1968) Dynamic response of the human cadaver head compared to a simple mathematical model. Proc. 12th Stapp Car Crash Conference, pp. 280-301. Society of Automotive Engineers, Warrendale, PA.

Hodgson, V. and Thomas, L. (1971) Comparison of head acceleration injury indices in cadaver skull fracture. Proc. 15th Stapp Car Crash Conference, pp. 190-206. Society of Automotive Engineers, Warrendale, PA.

Hubbard, R. P. (1971) Flexure of layered cranial bone. Journal of Biomechanics 4(4): 251-63.

Hubbard, R. P., Melvin, J. W. and Barodawala, I. T. (1971) Flexure of cranial sutures. Journal of Biomechanics 4(6): 491-6.

Irwin, A. and Mertz, H. (1997) Biomechanical basis for the CRABI and Hybrid III child dummies. Proc. 41st Stapp Car Crash Conference, pp. 261-272. Society of Automotive Engineers, Warrendale, PA..

James, H. E. (1999) Pediatric head injury: what is unique and different. Acta neurochirurgica. Supplementum. 73: 85-8.

Klinich, K., Hulbert, G. and Schneider, L. (2002) Estimating infant head injury criteria and impact response using crash reconstruction and finite element modeling. Stapp Car Crash Journal 46: 165-194.

Kraus, J. F., Rock, A. and Hemyari, P. (1990) Brain injuries among infants, children, adolescents, and young adults. American Journal of Diseases of Children 144(6): 684-91.

Kriewall, T., McPherson, F. and Tsai, A. (1981) Bending properties and ash content of fetal cranial bone. Journal of Biomechanics 14: 73-79.

Luerssen, T. (1993) General characteristics of neurologic injury. In Pediatric Trauma, M. Eichelberger, Mosby Year Book, Inc., St. Louis,.

Margulies, S. S. and Thibault, K. L. (2000) Infant skull and suture properties: measurements and implications for mechanisms of pediatric brain injury. Journal of Biomechanical Engineering 122(4): 364-71.

McElhaney, J., Roberts, V. and Hilyard, J. (1976) Handbook of Human Tolerance. Japan Automobile Research Institute, Tokyo,

McPherson, G. and Kriewall, T. (1980) The elastic modulus of fetal cranial Bone: a first step toward understanding of the biomechanics of fetal head molding. Journal of Biomechanics 13: 9-16.

Meirovitch, L. (2001) Fundamentals of Vibrations. McGraw-Hill, Boston.

Melvin, J. (1995) Injury Assessment Reference Values for the CRABI 6-Month Infant Dummy in a Rear-Facing Infant Restraint with Airbag Deployment. SAE 950872. Society of Automotive Engineers, Warrendale, PA.

Mertz, H. (1985). Biofidelity of the Hybrid III head, SAE 851245. Society of Automotive Engineers, Warrendale, PA.

Mertz, H., Irwin, A., Melvin, J. W., Stalnaker, R. L. and Beebe, M. S. (1989) Size, weight and biomechanical impact response requirements for adult size small female and large male dummies. In Automotive Frontal Impacts, pp. 133-144. Society of Automotive Engineers, Warrendale, PA.

Myers, B. S. (1997). An evaluation of a helmet standard for children, United States Consumer Product Safety Commission.**:** Republished in part in the U.S. Federal Register, 16 CFR Part 1203, 11711-11747, 1998.

Nightingale, R. W., McElhaney, J. H., Richardson, W. J. and Myers, B. S. (1996) Dynamic responses of the head and cervical spine to axial impact loading. Journal of Biomechanics 29(3): 307-18.

Ommaya, A., Yarnell, P., Hirsch, A. and Harris, E. (1967) Scaling of experimental data on cerebral concussion in sub-human primates to concussion threshold for man. Proc. 11th Stapp Car Crash Conference, pp. 73-80. Society of Automotive Engineers, Warrendale, PA.

Ono, K., Kikuchi, A., Nakamura, M., Kobayashi, H. and Nakamura, N. (1980) Human head tolerance to sagittal impact reliable estimation deduced from experimental head injury using subhuman primates and human cadaver skulls. Proc. 24th Stapp Car Crash Conference, pp. 103-160. Society of Automotive Engineers, Warrendale, PA.

Prasad, P. and Daniel, R. (1984) A biomechanical analysis of head, neck, and torso injuries to child surrogates due to sudden torso acceleration. Proc. 28th Stapp Car Crash Conference, pp. 25-40. Society of Automotive Engineers, Warrendale, PA.

Ridgway, E. B. and Weiner, H. L. (2004) Skull deformities. Pediatric Clinics of North America 51(2): 359-87.

Schneider, L., Lehman, R., Pflug, M. and Owings, C. (1986). Size and shape of the head and neck from birth to four years. UMTRI-86-2 University of Michigan Transportation Research Institute. Ann Arbor, MI.

Thibault, K. and Margulies, S. (1998) Age-dependent material properties of the porcine cerebrum: effect on pediatric inertial head injury criteria. Journal of Biomechanics 31: 1119-1126.

Thomas, L., Sezgin, Y., Hodgson, V., Cheng, L. and Gurdjian, E. (1968) Static deformation and volume changes in the human skull. Proc. 12th Stapp Car Crash Conference, pp. 260-270. Society of Automotive Engineers, Warrendale, PA.

Walker, L., Harris, E. and Pontius, U. (1973) Mass, volume, center of mass, and mass moment of inertia of head and head and neck of human body. Proc. 17th Stapp Car Crash Conference, pp. 525-537. Society of Automotive Engineers, Warrendale, PA.

APPENDIX

Table A1: Anthropomorphic data for infant cadaver head specimens with mandible attached.

		Specimen			6 month CRABI ¥
Specimen ID		P03	P05	P06	
Age (days after birth)		3	1	11	-
Head mass (gm)		491.5	666.5	701.9	2110
Body mass (gm)		1910	1881*	2583	7820
Head length (cm) ‡		10.3	10.8	11.2	15.6
Head breadth (cm) ‡		8.5	8.8	10.4	11.9
Head height (cm) §		7.5	8.8	9.2	-
facial length (cm) §		4.2	5.1	4.8	-
Bizygomatic diameter (cm) §		5.5	6.2	5.9	-
Anterior condyle	x (cm) §	-0.6	-0.7	-0.5	-
	z (cm) §	0.7	0.6	0.5	-
Posterior condyle	x (cm) §	-1.2	-1.4	-1.1	-
	z (cm) §	0.6	0.4	0.5	-
Center of condyle	x (cm)	-0.9	-1.0	-0.8	-
	z (cm)	0.7	0.5	0.5	-
Head Cg	x (cm)	-0.2	0.4	1.0	-
	z (cm)	-1.1	-2.9	-2.9	-
Head Iyy at Cg (gm*cm^2)		4813	5172	4850	-

* body mass without limbs, ‡ measurements using calipers, § measurements from CT data.
¥ CRABI anthropometry from Irwin and Mertz 1997
Coordinate system for Cg and condyle measurements: origin at superior margin of auditory meatus, positive x direction in anterior direction along Frankfort, z positive in inferior direction.
Head height: length from auditory meatus to top of head, facial length: length between nasion and gnathion,

Table A2: Regression results from cadaver head compression tests in different directions and velocities.

Compression direction	Velocity	Specimen	Measured velocity (mm/s)	Linear fit			Exponential fit		
				Stiffness (N/mm)	Low load Displacement (mm)	r^2	A (N)	B (mm^{-1})	r^2
Anterior-posterior	0.05 mm/s	P03	0.05	5.6	1.2	0.99	9.0	0.25	1.00
		P05	0.05	9.7	1.1	1.00	16.2	0.25	1.00
		P06	0.05	5.5	1.6	0.99	4.6	0.32	1.00
	1.0 mm/s	P03	1.0	26.7	1.6	0.99	22.0	0.34	1.00
		P05	1.0	13.5	1.3	0.99	20.6	0.25	1.00
		P06	1.0	22.1	1.5	1.00	27.7	0.27	1.00
	10 mm/s	P03	10	34.8	1.8	0.99	17.2	0.41	1.00
		P05	10	15.8	1.2	0.99	28.9	0.23	1.00
		P06	10	23.8	1.9	0.99	14.4	0.37	1.00
	50 mm/s	P03	67	35.4	1.5	0.99	20.0	0.43	1.00
		P05	64	15.4	0.7	0.99	44.3	0.19	1.00
Right-Left	0.05 mm/s	P03	0.05	9.8	1.0	1.00	17.9	0.25	1.00
		P05	0.05	6.8	1.2	0.99	8.2	0.30	1.00
		P06	0.05	7.2	0.7	0.98	24.3	0.17	0.99
	1.0 mm/s	P03	1.0	34.7	1.6	1.00	16.2	0.45	1.00
		P05	1.0	21.1	1.7	0.99	6.3	0.53	1.00
		P06	1.0	21.3	1.8	0.98	7.6	0.49	1.00
	10 mm/s	P03	10	44.7	1.6	0.99	20.0	0.46	1.00
		P05	10	25.4	1.7	0.99	9.0	0.50	1.00
		P06	10	34.9	1.7	0.99	15.4	0.45	1.00
	50 mm/s	P03	58	44.6	1.2	1.00	30.6	0.41	1.00
		P05	55	22.8	1.2	0.99	14.3	0.44	0.99

Table A3: Results from cadaver head drop tests onto different impact locations and at 2 different heights.

Approximate Drop height	Location	Specimen	Measured drop height (cm)	Head mass* (gm)	Peak acceleration (g)	Duration (msec)	HIC
15cm	Vertex	P03	15.9	415.3	64.5	13.7	64
		P05	14.6	601.1	37.3	26.0	29
		P06	14.6	646.7	41.3	23.9	28
	Occiput	P03	16.2	415.3	46.0	12.9	48
		P05	14.0	601.1	35.4	22.5	24
		P06	15.2	646.7	32.7	23.5	25
	Forehead	P03	15.2	415.3	49.5	12.9	55
		P05	15.2	601.1	26.1	22.6	17
		P06	14.6	646.7	26.3	23.4	20
	Right Parietal	P03	15.9	415.3	48.0	12.8	49
		P05	15.6	601.1	32.2	25.0	24
		P06	15.2	646.7	33.4	20.1	22
	Left Parietal	P03	15.9	415.3	41.0	13.0	39
		P05	15.9	601.1	37.2	19.1	27
		P06	14.1	646.7	32.1	20.8	22
30cm	Vertex	P03	30.8	415.3	112.4	11.7	205
		P05	30.5	601.1	57.1	22.1	71
		P06	30.5	646.7	74.6	20.1	96
	Occiput	P03	30.5	415.3	72.1	12.8	109
		P05	29.2	601.1	55.9	18.8	71
		P06	30.5	646.7	52.9	20.6	75
	Forehead	P03	30.5	415.3	82.1	12.0	179
		P05	31.1	601.1	38.0	22.1	38
		P06	29.2	646.7	43.1	20.7	47
	Right Parietal	P03	29.8	415.3	77.6	12.9	138
		P05	29.2	601.1	55.2	18.5	70
		P06	30.3	646.7	48.0	17.0	59
	Left Parietal	P03	30.5	415.3	61.9	12.3	113
		P05	29.8	601.1	52.6	17.4	71
		P06	29.7	646.7	46.1	18.0	64

* head mass was measured and tests were conducted with the mandible removed from the specimen.

Table A4: Coefficients and results of modeling cadaver head impact tests as a mass-spring system (see equation 3)

Approximate Drop height	Location	Specimen	k (N/mm)	predicted peak acceleration (g)	duration (msec)	r^2
15cm	Vertex	P03	37.9	54.3	10.4	0.79
		P05	26.1	35.9	15.1	0.83
		P06	24.7	33.7	16.1	0.78
	Occiput	P03	29.3	48.2	11.8	0.85
		P05	22.1	32.4	16.4	0.82
		P06	21.9	32.4	17.1	0.86
	Forehead	P03	39.2	54.2	10.2	0.85
		P05	27.0	37.3	14.8	0.75
		P06	21.6	31.6	17.2	0.84
	Right Parietal	P03	37.4	54.0	10.4	0.85
		P05	37.1	44.3	12.7	0.79
		P06	21.7	32.2	17.1	0.75
	Left Parietal	P03	34.0	51.5	10.9	0.79
		P05	33.1	42.2	13.4	0.80
		P06	28.1	35.3	15.1	0.83
30cm	Vertex	P03	70.9	103.6	7.6	0.82
		P05	30.3	56.0	14.0	0.79
		P06	36.8	59.5	13.2	0.77
	Occiput	P03	36.8	74.3	10.5	0.81
		P05	35.6	59.4	12.9	0.82
		P06	30.3	54.0	14.5	0.85
	Forehead	P03	62.9	97.0	8.0	0.89
		P05	30.7	56.9	13.9	0.71
		P06	23.4	46.4	16.5	0.78
	Right Parietal	P03	46.2	82.3	9.4	0.85
		P05	49.2	69.8	11.0	0.81
		P06	34.2	57.2	13.7	0.79
	Left Parietal	P03	42.4	79.7	9.8	0.80
		P05	51.0	71.8	10.8	0.79
		P06	35.0	57.3	13.5	0.82

Table A5: Coefficients and results of modeling cadaver head impact tests as a three parameter model (see equation 4).

Approximate Drop height	Location	Specimen	c (N*sec/mm)	k_2 (N/mm)	k_1 (N/mm)	predicted peak acceleration (g)	duration (msec)	r^2
15cm	Vertex	P03P	0.276	74.1	7.7	55.8	7.4	0.91
		P05P	0.187	55.0	8.3	34.9	11.0	0.93
		P06P	0.233	55.6	6.4	34.7	11.1	0.88
	Occiput	P03P	0.218	28.5	5.6	40.2	11.3	0.95
		P05P	0.141	36.6	9.7	30.5	12.9	0.93
		P06P	0.201	29.7	5.5	29.2	14.3	0.95
	Forehead	P03P	0.239	57.5	5.6	47.6	8.5	0.96
		P05P	0.093	49.4	9.7	27.4	15.2	0.97
		P06P	0.136	23.9	5.5	24.5	16.4	0.97
	Right Parietal	P03P	0.174	30.5	9.8	42.6	10.5	0.96
		P05P	0.136	62.2	6.8	31.1	12.7	0.98
		P06P	0.155	31.4	7.2	28.6	14.3	0.83
	Left Parietal	P03P	0.116	33.1	9.8	38.7	10.9	0.97
		P05P	0.166	41.8	6.8	32.4	12.5	0.94
		P06P	0.177	30.8	7.2	28.6	14.0	0.90
30cm	Vertex	P03P	0.345	131.7	7.7	97.0	5.7	0.92
		P05P	0.192	78.6	8.3	53.8	10.0	0.93
		P06P	0.301	110.2	6.4	64.0	8.3	0.89
	Occiput	P03P	0.217	40.8	5.6	60.2	9.8	0.90
		P05P	0.186	54.5	9.7	50.6	10.9	0.94
		P06P	0.254	47.3	5.5	48.9	11.7	0.95
	Forehead	P03P	0.363	68.6	5.6	79.4	7.6	0.97
		P05P	0.105	67.1	9.7	41.7	14.5	0.94
		P06P	0.147	22.8	5.5	35.3	16.3	0.84
	Right Parietal	P03P	0.227	66.9	9.8	72.5	7.8	0.95
		P05P	0.209	63.2	6.8	51.2	10.4	0.97
		P06P	0.183	26.6	7.2	41.4	14.6	0.87
	Left Parietal	P03P	0.165	36.8	9.8	60.0	10.0	0.93
		P05P	0.194	60.7	6.8	49.9	10.8	0.98
		P06P	0.189	42.5	7.2	44.6	12.5	0.96

Table A6: Results from CRABI head drop tests onto different impact locations and at 2 different heights.

Approximate Drop height	Location	Measured drop height (cm)	Head mass (gm)	Peak acceleration (g)	Duration (msec)	HIC
15cm	Vertex	14.0	2095.3	33.8	19.4	38
	Occiput	15.2	2095.3	39.5	17.6	48
	Forehead	16.5	2095.3	37.3	19.4	41
	Right Parietal	14.9	2095.3	66.8	11.0	76
	Left Parietal	15.2	2095.3	116.0	10.7	142
30cm	Vertex	29.2	2095.3	51.8	18.0	99
	Occiput	29.2	2095.3	61.6	15.6	126
	Forehead	29.2	2095.3	84.8	14.0	157
	Right Parietal	30.5	2095.3	144.9	9.9	301
	Left Parietal	30.5	2095.3	214.5	9.6	488

Table A7: Regression results from CRABI head compression tests in different directions and velocities.

Compression direction	Measured velocity (mm/s)	Linear fit			Exponential fit		
		Stiffness (N/mm)	Low load Displacement (mm)	r^2	A (N)	B (mm^{-1})	r^2
Anterior-posterior	0.05	18.5	0.3	1.00	274.5	0.06	1.00
	1.0	22.4	0.4	1.00	253.0	0.07	1.00
	10	26.2	0.4	1.00	279.2	0.07	1.00
	42	28.7	0.4	1.00	211.5	0.10	1.00
Right-Left	0.05	62.4	0.4	0.99	48.9	0.56	1.00
	1.1	82.9	0.4	0.99	108.3	0.41	1.00
	10	95.1	0.3	0.99	117.2	0.43	1.00
	31	95.7	0.3	0.99	124.4	0.44	1.00